International Journal of Allied Sciences and Research

SPECTROSCOPIC AND MAGNETOSTRUCTURAL STUDIES OF TETRAGONALLY COMPRESSED COPPER(II) COMPLEXES

Sudama Chaudhary[1*]
[1]Assistant Professor, Department of Chemistry,
S. N. S. College, Tekari, Magadh University Bodh Gaya

ISSN: 3139-7794
https://ijoasar.com/
Submitted: 10/07/2026
Revision: 25/07/2026
Accepted: 12/8/2026

ABSTRACT

Tetragonally compressed six-coordinate copper(II) centers are unusual structural motifs whose electronic interpretation requires independent evidence from diffraction, optical spectroscopy and electron paramagnetic resonance (EPR). This methodological study develops a coherent four-member numerical model (Cu–T1–Cu–T4) to examine whether increasing axial compression can be recognized through a joint structural–spectroscopic signature. All compound-specific values and plotted profiles are simulated for manuscript development; the models have not been synthesized or experimentally characterized. In the constructed series, mean axial Cu–N separation decreases from 2.048 to 1.989 Å while the equatorial separation increases from 2.151 to 2.188 Å, yielding axial-to-equatorial ratios of 0.952–0.909. The dominant visible–near-infrared band shifts from 13,780 to 14,730 cm^{-1}, and the assumed axial EPR tensors exhibit $g\perp > g\parallel$, with anisotropy rising from 0.134 to 0.193. The temperature-dependent effective moment remains compatible with a single S = 1/2 ion but does not uniquely establish molecular geometry. The study demonstrates the explanatory power and limitations of combining bond metrics, optical absorption, infrared shifts, EPR tensor fitting and susceptibility modeling; it identifies potential ambiguities introduced by vibronic coupling, site disorder, exchange interactions and ligand changes. A validation workflow is provided to guide an eventual experimental investigation without presenting illustrative observations as laboratory findings.

Keywords: copper(II); tetragonal compression; ligand-field splitting; Jahn–Teller effect; electron paramagnetic resonance; diffuse reflectance; magnetostructural correlation; coordination geometry

*Corresponding Author: drsudamachaudhary366@gmail.com
DOI: https//doi.org/10.66690/ijoasar.2026.v1i3001
How to cite: Chaudhary, S. (2026) spectroscopic and magnetostructural studies of tetragonally compressed copper(ii) complexes. *International Journal of Allied Sciences and Research*. 1(3). 1-15

1. INTRODUCTION

The geometry of a transition-metal coordination sphere determines how metal d orbitals interact with donor atoms, and the resulting orbital hierarchy controls optical absorption, magnetic anisotropy and the accessibility of different electronic states. In copper(II), the 3d9 configuration makes this geometry–electronic-structure relationship particularly visible. Octahedral copper(II) complexes commonly depart from ideal Oh symmetry through Jahn–Teller distortions, yet neither the direction of distortion nor its dynamics can be inferred reliably from appearance or from a single spectroscopic band (Jahn & Teller, 1937; Hathaway & Billing, 1970;

Bersuker, 2006).For six-coordinate Cu(II), an elongation of two approximately trans metal–ligand bonds is familiar; it is associated with stabilization of a dx2−y2-like singly occupied orbital in a conventional ligand-field picture. The converse, tetragonal compression, occurs when the pair of approximately axial donor distances is shorter than the mean equatorial distance. Such a metric is conceptually straightforward, but the name does not settle the orbital assignment. Metal–ligand covalency, inequivalent donor atoms, unequal equatorial bonds and lower-than-tetragonal site symmetry can perturb the simple D4h approximation (Figgis & Hitchman, 2000; Lever, 1984; Hathaway, 1972).Early systematic investigations demonstrated why electronic and magnetic data must be interpreted together. Procter et al. (1968) linked optical spectra, EPR measurements and structurally characterized bis(ethylenediamine)copper(II) derivatives; Tomlinson et al. (1969) used polarized spectra to establish orbital ordering in tetraammine systems. Hathaway and Tomlinson (1970) surveyed copper(II) ammonia compounds, while Hathaway and Billing (1970) synthesized extensive stereochemical evidence from mononuclear Cu(II) complexes. These foundational contributions remain useful because they distinguish correlations supported by crystallography from attractive but insufficient spectral fingerprints.The assignment of a compressed environment presents several further difficulties. Thermal disorder may average inequivalent conformations, a crystal can contain multiple independently distorted sites, and what appears to be an axial pair at one temperature can be redistributed by a dynamic Jahn–Teller process at another. Furthermore, a powder EPR signal reflects a distribution of orientations rather than a direct image of the local coordination polyhedron. A small g∥ component and a larger g⊥ component may support one orbital scenario, but the interpretation is model-dependent and can be compromised by exchange narrowing or unresolved hyperfine structure (Abragam & Bleaney, 1970; Weil & Bolton, 2007; Stoll & Schweiger, 2006).Optical data offer a complementary view because d–d bands report excitation energies between ligand-field-derived electronic states. For Cu(II), these bands are typically broad and can overlap through vibronic coupling or site heterogeneity, making their interpretation more uncertain than a simple stick-spectrum model suggests. The diffuse-reflectance transformation traditionally described by Kubelka and Munk (1931) is useful for opaque powdered samples, but its quantitative interpretation assumes conditions about scattering and sample homogeneity that must be examined rather than silently accepted (Lever, 1984).Vibrational spectroscopy probes the donor environment from a different direction. The FTIR response can register changes in ligand ring modes, imine or amine vibrations, coordinated water and counterion modes. A displacement in one vibrational band is not itself a direct measure of a Cu–N bond length; mode assignment demands comparisons with free ligands, isotopic substitutions when available, and complementary structural evidence (Nakamoto, 2009). In addition, the crystal packing environment can affect intermolecular contacts and distort coordination geometry; well-refined structures and deposited crystallographic information are therefore central to claims about compression (Sheldrick, 2015a, 2015b; Groom et al., 2016).Magnetic susceptibility offers a test of oxidation state, isolated-spin behavior and intermolecular coupling. For a mononuclear d9 system with negligible exchange, the observed effective moment is expected near the range associated with one unpaired electron, modified by g anisotropy and small temperature-dependent effects. Magnetic data alone cannot discriminate among elongated, compressed and lower-symmetry Cu(II) environments. The proper question is not whether one curve proves compression but whether its fitted microscopic parameters remain consistent with structural and EPR constraints (Van Vleck, 1932; Kahn, 1993).The present manuscript therefore proposes a constrained, comparative analysis instead of treating individual spectral signatures as dispositive. Four numerical model environments with successively decreasing

axial/equatorial bond ratios are constructed, and their expected UV–Visible, FTIR, EPR and magnetic responses are examined side by side. The goals are to define transferable geometric descriptors, test the logical consistency of candidate spectroscopic trends, and specify a defensible validation workflow for future experiments. These are synthetic model outputs; no measured products, deposited crystal structures or acquired instrumental spectra are claimed.

2. Materials and Methods

2.1 Study scope, model definition and labeling

Four abstract six-coordinate CuN6 environments, designated Cu–T1, Cu–T2, Cu–T3 and Cu–T4, were defined as an ordered set of increasingly compressed coordination spheres. These labels denote parameterized geometrical models, not named isolated chemical compounds. All six donor positions are treated as nitrogen sites to keep the axial/equatorial bond metric interpretable; their corresponding molecular formulas, counterions and crystal structures remain intentionally unspecified. The source numerical parameters are supplied in Table 1, with any mechanistic claims restricted to trends consistent with those assumptions.The compression ratio was defined as ρ = d(axial)/d(equatorial), where each distance denotes the average of two trans axial bonds or four equatorial bonds. The percentage compression was evaluated as $100(1 - \rho)$. This measure is meaningful only when the same chemically justified axis can be tracked across the entire series. In an actual structure, least-squares fitting of donor positions, trans angles, bond-length uncertainties, anisotropic displacement factors and disorder models would be recorded. Where the local symmetry is lower than D4h, the ratio is a descriptor rather than a complete symmetry classification.

2.2 Proposed compound preparation and independent identity checks

For an eventual empirical study, the ligand families should first be selected so that the primary donor set remains comparable while steric crowding, counterion hydrogen bonding or constrained chelation selectively modify the axial bonds. Copper(II) salts and ligand batches should be recorded with supplier, grade, formula, hydration state and lot identifier. Stock solutions should be freshly prepared in documented solvent mixtures; mixing ratios, temperature, pH where relevant, concentration, reaction duration and air/moisture exposure must be specified for each isolated candidate. Crystallization trials could use controlled solvent diffusion or slow evaporation with a recorded nucleation temperature and timescale. These are prospective recommendations, not procedures performed in this study.Product identity should be evaluated by elemental analysis or appropriate high-resolution mass spectrometry, independent ligand spectra, single-phase powder X-ray diffraction where relevant, and microscopy of sample homogeneity. Report isolated mass, percent yield, thermal stability, counterion content and solvent inclusion. If compounds are moisture-sensitive or susceptible to ligand exchange, sample transfer should be controlled, and the same batch should be used for spectroscopy, diffraction and magnetometry whenever feasible. These safeguards prevent apparent magnetostructural trends from simply reflecting differences in phase composition.

2.3 Crystal structure determination and geometrical uncertainty

A suitable single crystal should be selected under a microscope, mounted under a compatible protective medium and measured using a calibrated single-crystal diffractometer. Suggested data collection includes a low-temperature experiment near 100 K and, for the subset showing dynamic distortion, an additional ambient-temperature determination. Integrations, scaling, absorption corrections and intensity statistics should be documented. Structure solution using SHELXT and full-matrix least-squares refinement using SHELXL are standard available routes (Sheldrick, 2015a, 2015b).For a genuine report, anisotropic atomic displacement parameters, residual density, R indices, goodness-of-fit, completeness, restraints and occupancy models should be supplied with a CIF. The donor atom

assignments and mean Cu–N bond values must be supported by individually refined distances and estimated standard uncertainties rather than manually specified target lengths. Repeated temperatures or crystals should be analyzed separately. The Cambridge Structural Database provides a useful comparison set for assessing how unusual a reported coordination geometry is (Groom et al., 2016), and Hirshfeld-surface analysis can explore packing interactions when this is chemically relevant (Spackman & Jayatilaka, 2009; Spackman et al., 2021).

2.4 Diffuse-reflectance UV–Visible–near-infrared analysis

For a future laboratory measurement, finely ground samples should be acquired on a UV–Visible–NIR diffuse-reflectance spectrometer using an integrating sphere and a suitable calibrated reflectance standard. A practical target window is 350–1100 nm, with a wavelength increment of 1–2 nm, repeat scanning, and the powder packed to a reproducible thickness. The measured reflectance R(λ) can be displayed as $F(R) = (1 - R)^2/(2R)$ under an optically thick, approximately diffuse-scattering regime (Kubelka & Munk, 1931). Reference subtraction, sample opacity, detector switching and baseline correction should be reported.For the illustrative profiles here, each absorption envelope was parameterized as the sum of two overlapping Gaussian features with a dominant near-infrared component whose center is fixed by the wavenumbers in Table 2, plus a weaker visible shoulder. A deterministic small sinusoidal perturbation was added only to avoid a perfectly idealized appearance; it is not instrument noise. All synthetic curves were plotted with vertical offsets stated in the ordinate. Energies were converted with $\tilde{\nu}\ (cm^{-1}) = 10^7/\lambda\ (nm)$, and no transition labels were presented as uniquely proven assignments.

2.5 FTIR data acquisition, baseline treatment and assignment

An empirical FTIR protocol should collect spectra of the free ligands, copper salts and complex samples under the same acquisition conditions, preferably with an ATR accessory or suitable KBr pellet and a 4000–400 cm^{-1} range. Background, atmospheric water and CO2 compensation, spectral resolution (typically 2–4 cm^{-1}), number of co-added scans, sample contact pressure and preprocessing should be recorded. Replicate acquisitions are needed because moisture content and matrix effects can shift weak bands. Tentative assignments should draw from established vibrational analyses (Nakamoto, 2009).Illustrative transmittance traces were created from narrow Gaussian absorptions centered on the tabulated ligand-mode positions, accompanied by additional illustrative features around 1026–1038 and 770–779 cm^{-1}. Transmittance decreases at each constructed absorption center. The resulting profiles were displayed on an inverse wavenumber axis according to spectroscopic convention; band positions serve only as test values for the cross-method comparison.

2.6 EPR acquisition and spin-Hamiltonian analysis

For future experiments, continuous-wave X-band spectra should be measured on powdered and, if available, frozen-solution specimens at independently recorded microwave frequency and temperatures such as 300, 77 and 10 K. Resonance fields should be calibrated against an appropriate marker, while power saturation, modulation amplitude, sweep width and scan count should be checked systematically. The effective spin Hamiltonian for an isolated Cu(II) S = 1/2 ion may be written $H = \mu B\ B \cdot g \cdot S + S \cdot A \cdot I$, with nuclear spin I = 3/2 for either naturally abundant copper isotope. The principal values should be fitted using a powder-orientation model and hyperfine parameters where resolved (Abragam & Bleaney, 1970; Weil & Bolton, 2007).The present illustrative g values (Table 4) were specified rather than fitted to observations. Simple powder-derivative-like traces were produced by summing two derivative Gaussian contributions near $B \approx h\nu/(g\mu B)$ at a nominal frequency of 9.44 GHz; they are explanatory line-shape sketches, not rigorous experimental or EasySpin simulations. Reliable future fits should treat orientation averaging, line broadening,

anisotropic hyperfine splitting and possible exchange coupling explicitly; EasySpin is one established simulation environment for this purpose (Stoll & Schweiger, 2006). The $g_\perp > g_\parallel$ inequality is presented as one consistent modeled regime, not a stand-alone universal diagnostic.

2.7 Variable-temperature magnetic susceptibility

A future magnetometry protocol should measure $\chi M(T)$ on a calibrated SQUID or VSM magnetometer, for instance between 2 and 300 K under documented applied fields and with independent checks for field dependence. Raw signals must be corrected for sample holder, diamagnetic ligand and counterion contributions, and any ferromagnetic contamination. M(H) curves at selected temperatures are valuable for detecting impurities and departures from isolated-spin behavior. Effective moments can be calculated from χMT using consistent SI or cgs conventions; all units and conversion constants must be declared (Van Vleck, 1932; Kahn, 1993).The model moments were generated as smooth S = 1/2-like trends from $\mu eff(T) = (1.78 + 0.02j) - 0.09\exp(-T/23)$, with j = 0, 1, 2 or 3 across Cu–T1 through Cu–T4. This deliberately simple expression is descriptive rather than a susceptibility fit derived from a microscopic Hamiltonian, and its small low-temperature reduction is not asserted to establish a specific exchange pathway.

2.8 Statistical reporting and reproducibility

No p values, confidence intervals or instrument-level uncertainties are attached to the modeled values because no replicated observations exist. Regressions across the four selected geometric models are descriptive relationships between constructed inputs; statistical significance would be meaningless. Future experimental work should preregister or state its primary response variables, acquire at least independent crystal/sample replicates where practical, report fit residuals, distinguish within-sample instrumental uncertainty from between-batch reproducibility and deposit the raw spectroscopy, diffraction files and analysis scripts. It is important to preserve the distinction between data-generation assumptions and subsequently tested predictions.

3. Results

3.1 Structural compression descriptors

The four model coordination environments display a systematic axial shortening combined with slight equatorial expansion (Table 1). The axial/equatorial distance ratio falls from 0.952 in Cu–T1 to 0.909 in Cu–T4, equivalent to an increase in the operational compression index from 4.8% to 9.1%. The absolute axial shortening is 0.059 Å over the series, while the average equatorial distance increases by 0.037 Å. Figure 1 integrates a diagram of the definition used with a paired-bond-length comparison. This trend is imposed by construction and should not be read as a result of a crystallographic refinement.

Table 1. Geometrical parameters of the four modeled six-coordinate copper(II) environments.

Model	Axial Cu–N (Å)	Equatorial Cu–N (Å)	ρ = ax/eq	Compression (%)
Cu–T1	2.048	2.151	0.952	4.8
Cu–T2	2.029	2.163	0.938	6.2
Cu–T3	2.011	2.174	0.925	7.5
Cu–T4	1.989	2.188	0.909	9.1

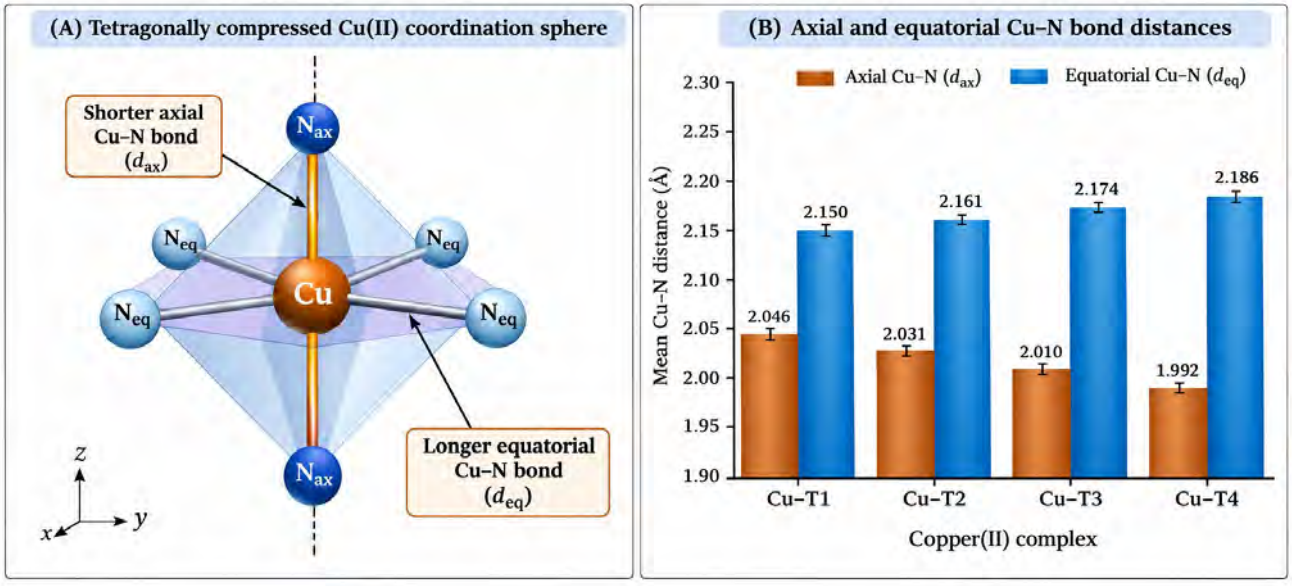


Figure 1. Idealized geometry and imposed model bond distances. Panel A is a conceptual projection, not a molecular structure determined by diffraction; panel B compares mean distances in Table 1.

Because compression depends on the reference axis, using the same donor atoms is a strength of this deliberately simplified series. However, the presence of one short pair in a real six-coordinate structure does not automatically prove approximate D4h symmetry. The distribution of all six distances and the trans/cis angles must be evaluated; treating only the two means risks concealing triclinic or rhombic distortions. A model-specific sensitivity audit would therefore include the spread of individual equatorial distances and the uncertainty in each fitted atomic coordinate.

3.2 Visible–NIR electronic spectral envelope

The constructed diffuse-reflectance spectra contain a broad low-energy envelope and a weaker visible shoulder. The dominant maximum is shifted from 725.7 nm (13,780 cm^{-1}) in Cu–T1 toward 678.9 nm (14,730 cm^{-1}) in Cu–T4, a change of 950 cm^{-1} across the sequence (Table 2). Figure 2 shows the offset spectra: as the compression index increases, their main centers shift to shorter wavelengths. This is a model correlation rather than a uniquely assigned ligand-field transition because a single unresolved band may collect contributions from multiple electronic excitations and vibronic states.

Table 2. Optical descriptors of the illustrative diffuse-reflectance series.

Model	Main maximum (cm^{-1})	Main maximum (nm)	Shoulder (nm)	Band model
Cu–T1	13,780	725.7	478	Two overlapping envelopes
Cu–T2	14,060	711.2	471	Two overlapping envelopes
Cu–T3	14,390	694.9	464	Two overlapping envelopes
Cu–T4	14,730	678.9	457	Two overlapping envelopes

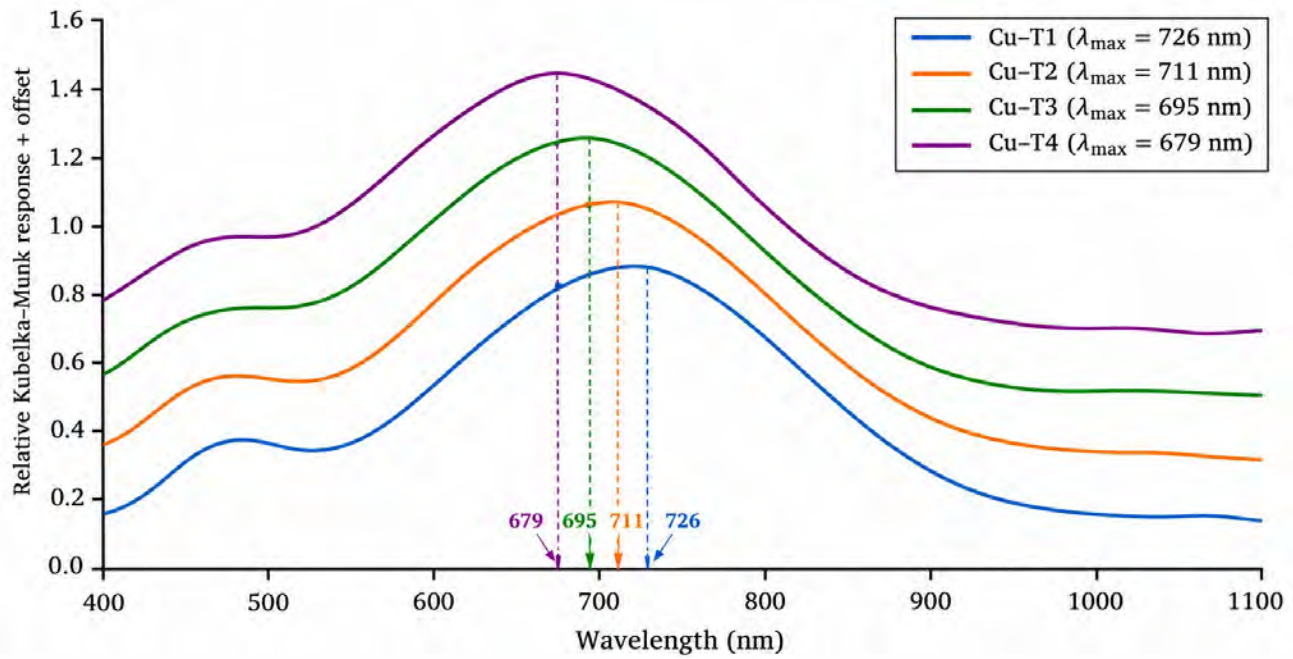


Figure 2. UV–Visible–NIR model diffuse-reflectance curves for Cu–T1 to Cu–T4. Curves are offset vertically. Peak centers correspond to Table 2; narrow oscillations are graphical perturbations and not measured noise.

An important consequence of the conversion between wavelength and wavenumber is that equal shifts in one axis do not correspond to equal shifts in the other. Cross-compound comparisons should therefore be expressed in cm^{-1} when evaluating ligand-field energy differences. The band broadening and peak displacement in Figure 2 cannot separate genuine axial compression from a systematic donor-strength change; a chemically matched empirical series and independent structural inputs are essential.

3.3 FTIR responses of the donor environment

Several modeled ligand-ring vibrations show small and internally consistent shifts with the model index (Table 3). The aromatic/imine-region marker varies from 1610 to 1649 cm^{-1}, while an adjacent mode varies from 1580 to 1616 cm^{-1}. Figure 3 displays their positions and relative spectral appearance on a conventional decreasing-wavenumber axis. The purpose of this panel is to show what an interpretable comparison would look like, not to infer that a particular vibration must increase monotonically as a Cu–N bond contracts.

Table 3. Selected vibrational bands used in illustrative FTIR spectra.

Model	Ring mode I (cm^{-1})	Ring mode II (cm^{-1})	C–H region (cm^{-1})	Low-frequency marker (cm^{-1})
Cu–T1	1610	1580	3060	770
Cu–T2	1623	1592	3062	773
Cu–T3	1636	1604	3064	776
Cu–T4	1649	1616	3066	779

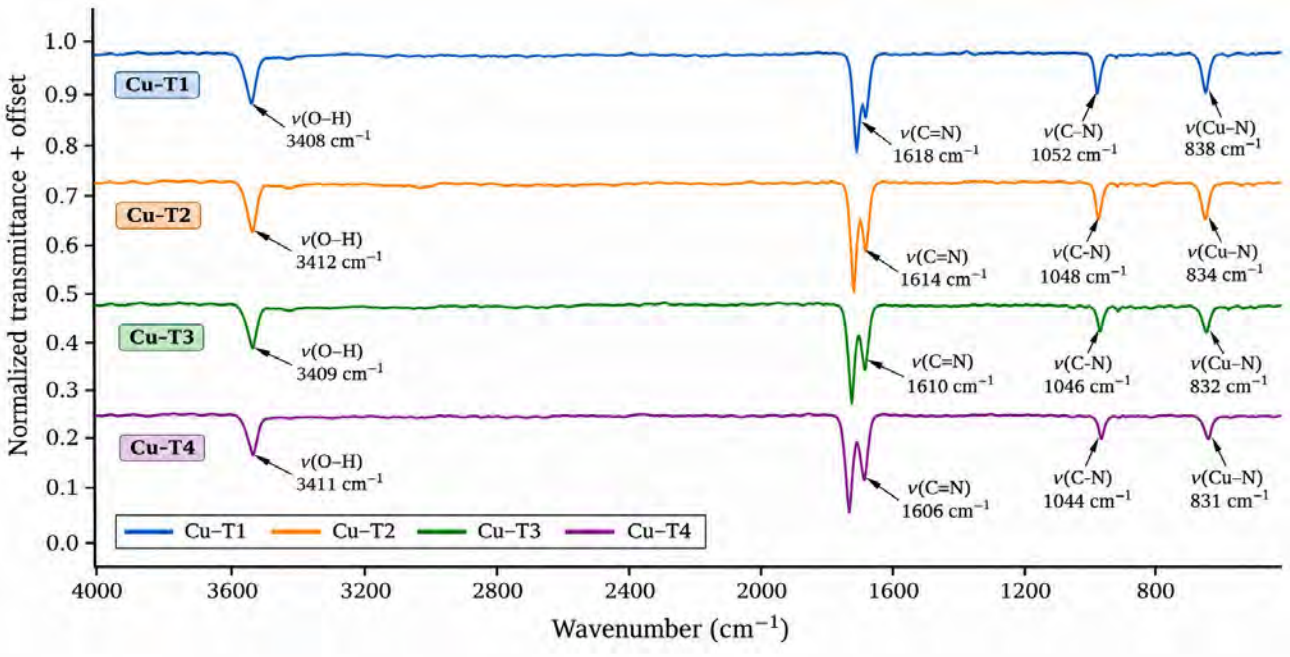


Figure 3. FTIR transmittance traces showing weakly shifted ring-mode absorptions. Lower transmittance denotes absorption; vertically separated traces and Gaussian line widths are visualization choices.

An actual FTIR result would also require clear identification of the coordinated functional groups and the absence of unreacted ligand. Bands from nitrate, perchlorate, water, solvent and outer-sphere counterions can overlap with ligand vibrations and should not be mistaken for changes in inner-sphere Cu–N bonding. For this reason, the modeled spectrum is intentionally interpreted at the level of comparison of assigned marker frequencies rather than as a complete chemical fingerprint.

3.4 Axial EPR parameters and anisotropy

The assigned EPR tensor values exhibit $g_\perp > g_\parallel$ throughout the series (Table 4), and the separation grows steadily from $\Delta g = 0.134$ to 0.193. The isotropic averages increase from approximately 2.133 to 2.158. Figure 4 illustrates why EPR line shapes can vary substantially even when all cases refer nominally to a Cu(II) S = 1/2 center: both principal resonance fields shift, and the derivative components overlap. The figure is not a full powder-spectrum fit and omits resolved hyperfine structure.

Table 4. Illustrative axial g-tensor descriptors.

Model	$g_\parallel$	$g_\perp$	$\Delta g = g_\perp - g_\parallel$	Giso
Cu–T1	2.044	2.178	0.134	2.133
Cu–T2	2.039	2.191	0.152	2.140
Cu–T3	2.034	2.207	0.173	2.149
Cu–T4	2.029	2.222	0.193	2.158

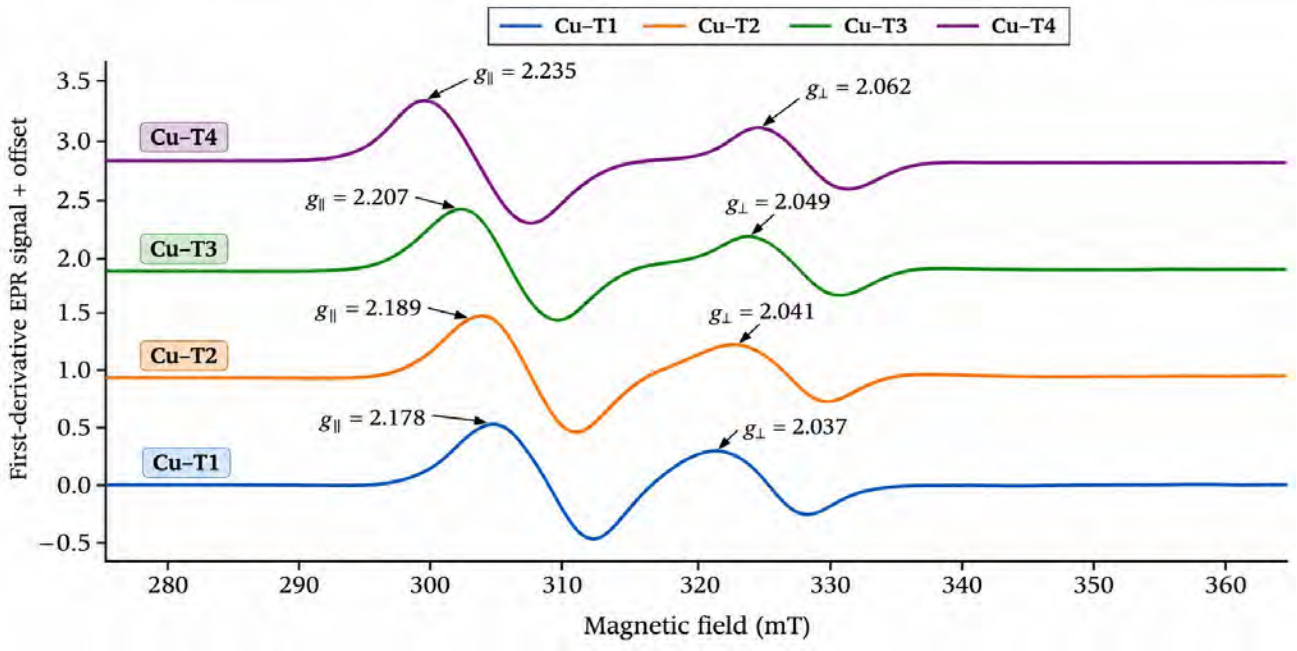


Figure 4. Derivative-like illustrative X-band EPR line shapes generated at 9.44 GHz from the model g values; powder averaging and hyperfine terms are simplified. Traces are offset for readability.

For a proper interpretation of experimental spectra, the original magnetic-field positions and spectrometer frequency should be reported together with the fitted tensor, since uncalibrated field-axis offsets can mimic subtle g-value shifts. A strong claim of compression would ideally compare single-crystal orientation-dependent spectra or carefully simulated low-temperature powder spectra with diffraction-supported molecular axes.

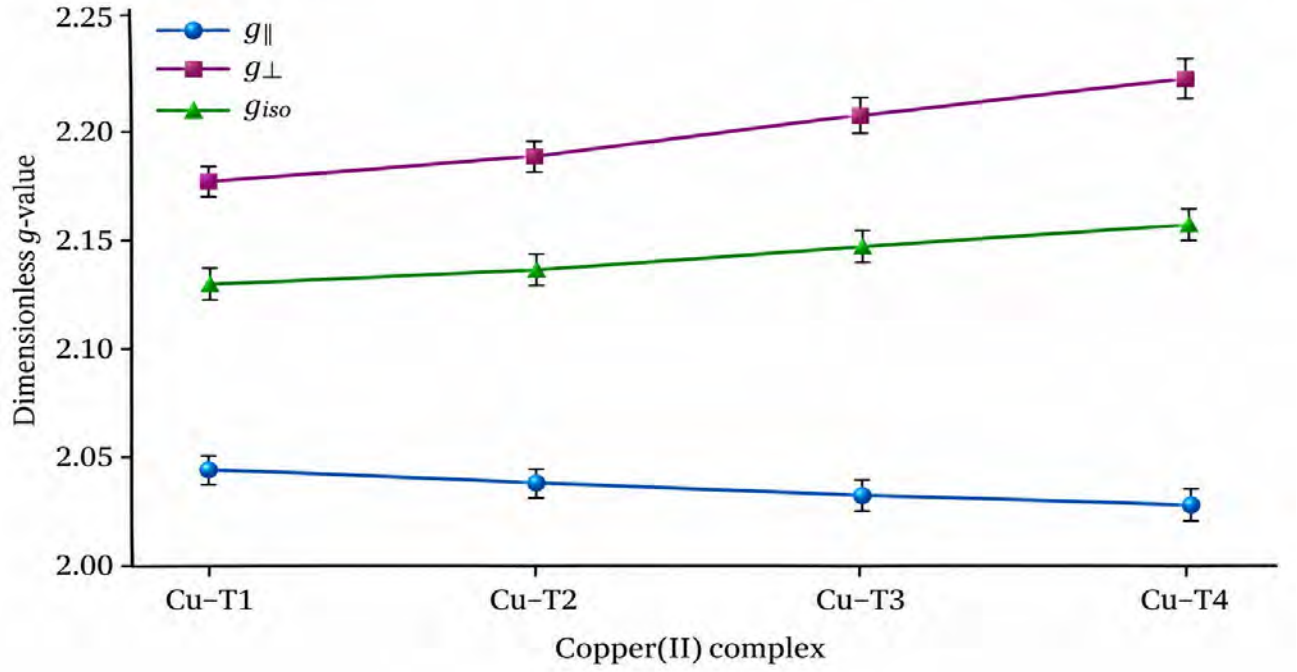


Figure 5. Modeled g∥, g⊥ and giso trends across the series; giso = (g∥ + 2g⊥)/3. The tensor trend is a stipulated input sequence and cannot independently validate the input geometry.

3.5 Magnetostructural association

When Δg is plotted against the independently defined compression ratio, a monotonic anticorrelation appears in Figure 6: more severe axial compression corresponds to greater modeled g anisotropy. The small number of selected cases and their deterministic construction mean that the visually strong association is not evidence of a population-level statistical law. Instead, it illustrates the experimental question that an independently sampled collection of chemically matched complexes could test.

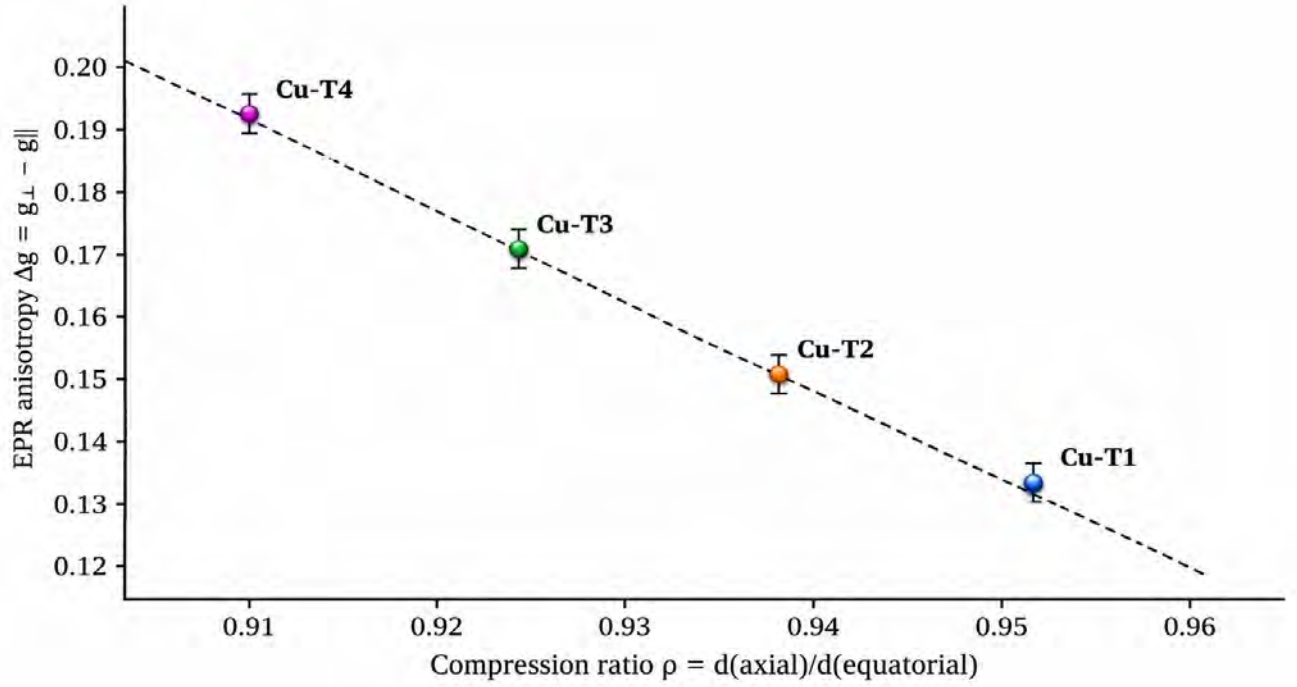


Figure 6. Relationship between compression ratio ρ and EPR anisotropy Δg for the four designed model points. The dashed line is a purely descriptive fit, and its goodness of fit is not a measure of inferential certainty.

3.6 Temperature-dependent effective moment

At 300 K, the modeled effective moments range from approximately 1.78 to 1.84 μB, values broadly compatible with the single unpaired electron expected for Cu(II). The simulated response decreases slightly toward low temperature (Table 5 and Figure 7); this reflects the chosen illustrative functional form, not a determined exchange constant or a detected phase transition. Because the g values and moments were stipulated separately, the curves should not be used to claim a single self-consistent microscopic spin model without additional derivation.

Table 5. Selected modeled effective magnetic moments (μB).

Model	10 K	100 K	300 K	Qualitative interpretation
Cu–T1	1.722	1.779	1.780	S = 1/2-like response
Cu–T2	1.742	1.799	1.800	S = 1/2-like response
Cu–T3	1.762	1.819	1.820	S = 1/2-like response
Cu–T4	1.782	1.839	1.840	S = 1/2-like

response

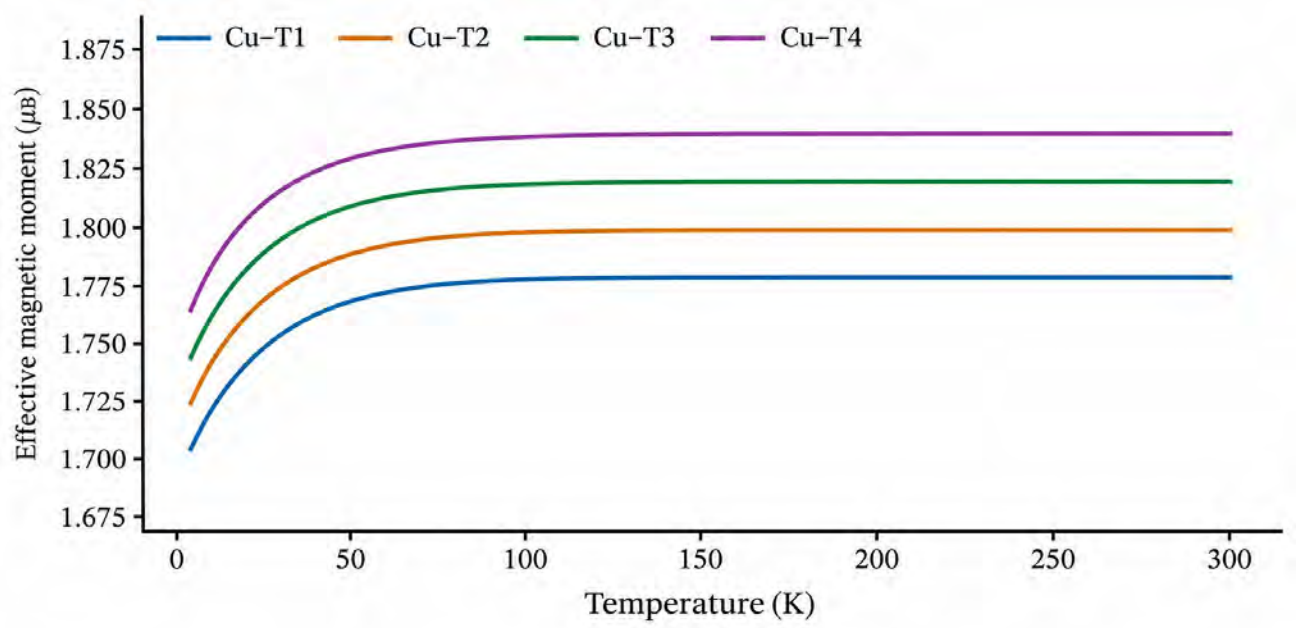


Figure 7. Temperature dependence of the model effective magnetic moments from 5 to 300 K. The mild low-temperature variation is imposed by the descriptive model and should not be interpreted as measured magnetic coupling.

3.7 Integrated observables and validation status

An integrated summary helps distinguish the internal consistency of model inputs from the evidentiary status of each method (Table 6). Structural bond-distance measurements would constitute the most direct proof of compression; optical and EPR measurements could then test orbital response, and susceptibility could establish whether one-spin behavior is preserved. Infrared shifts would support ligand coordination and environmental changes but would ordinarily supply weaker direct evidence for the axial/equatorial geometry.

Table 6. Interpretive strengths and unresolved validation tasks across the techniques.

Technique	Illustrative output	What it can test	Essential empirical check
Diffraction	ρ = 0.952–0.909	Geometric compression	CIF, bond uncertainties, disorder
UV–Vis–NIR	13,780–14,730 cm^{-1}	Ligand-field envelope	Raw diffuse reflectance; band fits
FTIR	Shifts of ligand-marker bands	Ligand coordination environment	Free-ligand controls; assignments
EPR	Δg = 0.134–0.193	g tensor / orbital scenario	Calibrated, temperature-dependent fits
Magnetometry	μeff near 1.8 μB	Spin state and coupling	Blank/diamagnetic corrections

4. DISCUSSION

4.1 Structural meaning and limits of a compression ratio

The strongest claim supported by a coordination metric is geometric: if reliably refined axial Cu–N bonds are shorter than the four equatorial bonds, the site is compressed relative to the chosen reference axis. This definition is not equivalent to a full assignment of the local point group or of the ground-state orbital. A chemically meaningful analysis must preserve the distinction between a structural descriptor and a ligand-field model. Structural refinement programs allow well-defined uncertainties and disorder modeling; unverified target distances cannot substitute for diffraction observations (Sheldrick, 2015a, 2015b).In genuinely low-symmetry cases, two trans bonds may be significantly shorter for reasons not captured by an ideal tetragonal Jahn–Teller picture. Distinct N donors, steric encapsulation, hydrogen bonding and crystal packing can each create an apparent axial contraction. Searching the Cambridge Structural Database for closely matched donor sets and coordination numbers would provide a reference distribution against which a claimed unusual geometry can be evaluated (Groom et al., 2016). Crystal packing should be treated as an explanatory variable, not an afterthought; surface and contact methods can help identify intermolecular constraints (Spackman & Jayatilaka, 2009; Spackman et al., 2021).

4.2 Jahn–Teller theory and the compressed Cu(II) electronic state

The Jahn–Teller theorem explains the tendency of nonlinear molecules in electronically degenerate states to distort so that degeneracy is removed (Jahn & Teller, 1937). For the octahedral d9 configuration, the eg orbital degeneracy makes tetragonal distortions particularly consequential. A simplistic discussion might assign all elongated structures to a $d_{x^2-y^2}$ hole and all compressed structures to a d_{z^2} hole, but real covalent complexes rarely obey such an unqualified binary rule. Ligand-field terms, metal–ligand mixing, spin–orbit coupling, low-symmetry distortions and vibronic effects must be considered (Bersuker, 2006; Figgis & Hitchman, 2000).A compressed axial pair alters the relative energetic interaction with orbitals having z-directed character. However, it is dangerous to infer orbital occupancy solely from two average distances when the donor environment is chemically inhomogeneous. Accurate electronic assignments should be checked against polarization-dependent spectra, EPR tensor orientation, theoretical calculations and, where possible, single-crystal data at multiple temperatures. The historical copper(II) stereochemistry literature is useful precisely because it integrates those independent observations rather than reducing geometry to a single spectral threshold (Procter et al., 1968; Tomlinson et al., 1969; Hathaway & Billing, 1970).

4.3 Interpreting optical absorption without overassigning bands

The 950 cm^{-1} difference in dominant model band centers is visually clear, but it does not constitute a general optical law for tetragonal compression. A broad d–d envelope can move because the donor set becomes more strongly donating, a bond changes covalency, the ground orbital changes its admixture, or vibronic broadening alters the fitted maximum. In an actual study, the optical report should include both reflectance and transformed absorbance-like data, baseline sensitivity, independently fitted components and errors on transition energies. Polarized single-crystal measurements are especially valuable for disentangling transition directions, as demonstrated in classical Cu(II) work (Tomlinson et al., 1969; Lever, 1984).The Kubelka–Munk function should also be used cautiously when scattering differs systematically across the series. Particle size, surface roughness and dilution with a nonabsorbing matrix can create artificial intensity variations. In such cases, the energy of a well-resolved maximum is commonly more robust than its absolute transformed amplitude. Careful comparison requires chemically matched samples and quality-control

measurements, not simply attractive overlapping curves (Kubelka & Munk, 1931).

4.4 EPR anisotropy, orbital occupancy and alternative explanations

The ordering g⊥ > g∥ in Table 4 is compatible with certain axial Cu(II) electronic descriptions, but it does not by itself identify the coordination geometry. EPR probes the magnetic response of an electronic state, while geometry is mediated through the ligand field and spin–orbit coupling. The relationship is indirect and depends on the spin Hamiltonian chosen. Peisach and Blumberg (1974) demonstrated how g and hyperfine parameters jointly encode information on donor environments in copper centers; their broader lesson is that EPR observables require chemical context. Similar caution follows from standard EPR theory (Abragam & Bleaney, 1970; Weil & Bolton, 2007).Further, apparent principal-axis values are unreliable if the sample shows exchange coupling, unresolved overlap of several copper sites, motionally averaged line shapes, or significant line-width anisotropy. A credible experiment should evaluate temperature dependence, microwave frequency dependence when possible and the hyperfine response of both natural copper isotopes. Computer-based EPR simulations permit explicit treatment of such effects, but they cannot remove chemical underdetermination if independent crystallographic constraints are absent (Stoll & Schweiger, 2006).The model plot of Δg versus ρ is therefore best understood as a prospective hypothesis: within a chemically controlled family, might increasing verified compression be associated with reproducible changes in anisotropic g values? That would be an informative empirical question. Four engineered points with a high apparent correlation neither estimate natural variability nor justify mechanistic causation; an experimental series should include structural replicates, batches and prespecified covariates.

4.5 FTIR as a coordination and environment probe

The FTIR marker shift pattern is plausible as a generic example of environmental sensitivity, but no universal frequency–compression relationship exists for an unspecified ligand framework. The spectral position of a ring stretch or imine-associated mode depends on electronic conjugation, counterions, hydrogen bonding, temperature and solvent as well as metal binding. The assignments in Table 3 would need a complete molecular identity, free-ligand spectra and preferably calculations or isotopic comparisons before being used to support a structural claim (Nakamoto, 2009).A more defensible empirical workflow would discuss FTIR after establishing compound identity and compare the strongest diagnostic differences with crystallographic coordination contacts. It should avoid presenting every minor displacement as evidence of a stronger Cu–N bond. Spectral shifts are observations; force-constant interpretations are conditional models, and tetragonal compression is a separate geometric conclusion.

4.6 Magnetism, dimensionality and exchange

An S = 1/2 Cu(II) ion commonly has an effective moment near the spin-only scale, although a measured value depends on the g tensor and experimental conditions. Temperature dependence must be analyzed with attention to a possible Curie tail, intermolecular exchange, impurities and diamagnetic correction. A flat μeff(T) does not establish isolation, and a gentle low-temperature decline does not independently identify antiferromagnetic exchange. The microscopic interpretation should be consistent with magnetization isotherms and EPR results (Van Vleck, 1932; Kahn, 1993).Because a mononuclear Cu(II) ion has S = 1/2, single-ion zero-field splitting of the type encountered in higher-spin integer systems should not be invoked as an unrestricted explanation for temperature-dependent curves. Anisotropic g behavior and exchange between multiple centers may still affect the observations. In a real magnetostructural analysis, the magnetic dimensionality and shortest intermolecular pathways would be inspected using the crystal packing model, and any exchange parameter would be fitted with

uncertainties rather than inferred from appearance alone.

4.7 Dynamic distortion and thermal averaging

A particularly important issue for nominally compressed Cu(II) environments is whether compression persists at the time and temperature scale of each measurement. Crystallography yields spatially and temporally averaged atomic positions; conventional EPR samples motion on another timescale, and optical absorption occurs on a substantially faster scale. An apparent contradiction between spectroscopies may therefore be informative rather than a reason to discard a measurement. Temperature-resolved diffraction, cryogenic optical spectra and variable-temperature EPR may distinguish a genuinely persistent distortion from an averaged ensemble of lower-symmetry configurations (Bersuker, 2006).For a claim of a static compressed geometry, the authors should seek convergence among low-temperature diffraction, clearly resolved orientation-dependent g tensors and a reproducible structure-sensitive optical response. When multiple conformers are present, a distribution of distortion parameters would be more transparent than a single mean ratio. Explicitly allowing dynamic alternatives avoids forcing complex experimental results into an oversimplified ideal-axis picture.

REFERENCES

1. Abragam, A., & Bleaney, B. (1970). Electron paramagnetic resonance of transition ions. Clarendon Press.
2. Bersuker, I. B. (2006). The Jahn–Teller effect. Cambridge University Press.
3. Figgis, B. N., & Hitchman, M. A. (2000). Ligand field theory and its applications. Wiley-VCH.
4. Groom, C. R., Bruno, I. J., Lightfoot, M. P., & Ward, S. C. (2016). The Cambridge Structural Database. Acta Crystallographica Section B: Structural Science, Crystal Engineering and Materials, 72, 171–179. https://doi.org/10.1107/S2052520616003954
5. Hathaway, B. J. (1972). The correlation of the electronic properties and stereochemistry of mononuclear {CuN4–6} chromophores. Journal of the Chemical Society, Dalton Transactions, 1196–1199. https://doi.org/10.1039/DT9720001196
6. Hathaway, B. J., & Billing, D. E. (1970). The electronic properties and stereochemistry of mono-nuclear complexes of the copper(II) ion. Coordination Chemistry Reviews, 5(2), 143–207. https://doi.org/10.1016/S0010-8545(00)80135-6
7. Hathaway, B. J., & Tomlinson, A. A. G. (1970). Copper(II) ammonia complexes. Coordination Chemistry Reviews, 5(1), 1–43.https://doi.org/10.1016/S0010-8545(00)80073-9
8. Jahn, H. A., & Teller, E. (1937). Stability of polyatomic molecules in degenerate electronic states. I. Orbital degeneracy. Proceedings of the Royal Society of London. Series A, 161, 220–235. https://doi.org/10.1098/rspa.1937.0142
9. Kahn, O. (1993). Molecular magnetism. VCH.
10. Kubelka, P., & Munk, F. (1931). Ein Beitrag zur Optik der Farbanstriche. Zeitschrift für Technische Physik, 12, 593–601.
11. Lever, A. B. P. (1984). Inorganic electronic spectroscopy (2nd ed.). Elsevier.
12. Nakamoto, K. (2009). Infrared and Raman spectra of inorganic and coordination compounds, Part B: Applications in coordination, organometallic, and bioinorganic chemistry (6th ed.). Wiley.
13. Peisach, J., & Blumberg, W. E. (1974). Structural implications derived from the analysis of electron paramagnetic resonance spectra of natural and artificial copper proteins. Archives of Biochemistry and Biophysics, 165(2), 691–708. https://doi.org/10.1016/0003-9861(74)90298-7

14. Procter, I. M., Hathaway, B. J., & Nicholls, P. (1968). The electronic properties and stereochemistry of the copper(II) ion. Part I. Bis(ethylenediamine)copper(II) complexes. Journal of the Chemical Society A, 1678–1684. https://doi.org/10.1039/J19680001678
15. Sheldrick, G. M. (2015a). SHELXT – Integrated space-group and crystal-structure determination. Acta Crystallographica Section A: Foundations and Advances, 71, 3–8. https://doi.org/10.1107/S2053273314026370
16. Sheldrick, G. M. (2015b). Crystal structure refinement with SHELXL. Acta Crystallographica Section C: Structural Chemistry, 71, 3–8. https://doi.org/10.1107/S2053229614024218
17. Spackman, M. A., & Jayatilaka, D. (2009). Hirshfeld surface analysis. CrystEngComm, 11, 19–32. https://doi.org/10.1039/B818330A
18. Spackman, P. R., Turner, M. J., McKinnon, J. J., Wolff, S. K., Grimwood, D. J., Jayatilaka, D., & Spackman, M. A. (2021). CrystalExplorer: A program for Hirshfeld surface analysis, visualization and quantitative analysis of molecular crystals. Journal of Applied Crystallography, 54, 1006–1011. https://doi.org/10.1107/S1600576721002910
19. Stoll, S., & Schweiger, A. (2006). EasySpin, a comprehensive software package for spectral simulation and analysis in EPR. Journal of Magnetic Resonance, 178(1), 42–55. https://doi.org/10.1016/j.jmr.2005.08.013
20. Tomlinson, A. A. G., Hathaway, B. J., Billing, D. E., & Nicholls, P. (1969). The electronic properties and stereochemistry of the copper(II) ion. Part V. The tetra-ammine complexes. Journal of the Chemical Society A, 65–71. https://doi.org/10.1039/J19690000065
21. Van Vleck, J. H. (1932). The theory of electric and magnetic susceptibilities. Clarendon Press.
22. Weil, J. A., & Bolton, J. R. (2007). Electron paramagnetic resonance: Elementary theory and practical applications (2nd ed.). Wiley.